2015

Molecular dynamics simulation on generalized stacking fault energies of FCC metals under preloading stress

Liang Zhang
University of Wollongong, lz592@uowmail.edu.au

Cheng Lu
University of Wollongong, chenglu@uow.edu.au

A Kiet Tieu
University of Wollongong, ktieu@uow.edu.au

Xing Zhao
University of Wollongong, xz920@uowmail.edu.au

Linqing Pei
University of Wollongong, lp115@uowmail.edu.au

See next page for additional authors

Publication Details

Zhang, L., Lu, C., Tieu, K., Zhao, X., Pei, L. & Michal, G. (2015). Molecular dynamics simulation on generalized stacking fault energies of FCC metals under preloading stress. Chinese Physics B, 24 (8), 088106-1-088106-8.

Molecular dynamics simulation on generalized stacking fault energies of FCC metals under preloading stress

Abstract
Molecular dynamics (MD) simulations are performed to investigate the effects of stress on generalized stacking fault (GSF) energy of three fcc metals (Cu, Al, and Ni). The simulation model is deformed by uniaxial tension or compression in each of [111], [11-2], and [1-10] directions, respectively, before shifting the lattice to calculate the GSF curve. Simulation results show that the values of unstable stacking fault energy (γusf), stable stacking fault energy (γsf), and unstable twin fault energy (γutf) of the three elements can change with the preloaded tensile or compressive stress in different directions. The ratio of γsf/γusf, which is related to the energy barrier for full dislocation nucleation, and the ratio of γutf/γusf, which is related to the energy barrier for twinning formation are plotted each as a function of the preloading stress. The results of this study reveal that the stress state can change the energy barrier of defect nucleation in the crystal lattice, and thereby can play an important role in the deformation mechanism of nanocrystalline material.

Keywords
under, preloading, stress, energies, dynamics, fault, simulation, stacking, generalized, molecular, fcc, metals

Disciplines
Engineering | Science and Technology Studies

Publication Details
Zhang, L., Lu, C., Tieu, K., Zhao, X., Pei, L. & Michal, G. (2015). Molecular dynamics simulation on generalized stacking fault energies of FCC metals under preloading stress. Chinese Physics B, 24 (8), 088106-1-088106-8.

Authors
Liang Zhang, Cheng Lu, A Kiet Tieu, Xing Zhao, Linqing Pei, and Guillaume Michal

Molecular Dynamics Simulation on Generalized Stacking Fault Energies of FCC Metals under Preloading Stress

Liang Zhang, Cheng Lu, Kiet Tieu, Xing Zhao, Linqing Pei, Guillaume Michal

School of Mechanical, Materials and Mechatronic Engineering, University of Wollongong, Wollongong, NSW 2522, Australia

Abstract: Molecular dynamics (MD) simulations were performed to investigate the effect of stress on generalized stacking fault (GSF) energy of three fcc metals (Cu, Al and Ni). The simulation model was deformed by uniaxial tension or compression in [1 1 1], [1 1 -2] and [1 -1 0] direction respectively before shifting the lattice to calculate the GSF curve. Simulation results show that, the unstable stacking fault energy (γ_{usf}), stable stacking fault energy (γ_{sf}) and unstable twin fault energy (γ_{utf}) of the three elements can change with the preloaded tensile or compressive stress in different directions. The ratio of γ_{sf}/γ_{usf}, which is associated with the energy barrier for full dislocation nucleation and the ratio of $\gamma_{utf}/\gamma_{usf}$, which is related to the energy barrier for twinning formation were plotted as a function of the preloading stress. The results of this study revealed that the stress state can change the energy barrier of defects nucleation in the crystal lattice, and thereby can play an important role in the deformation mechanisms of nanocrystalline materials.

Keywords: Molecular dynamics, EAM, Generalized stacking fault

PACS: 81.07.Nb, 81.07.Bc, 81.40.Vw, 81.40.Jj

1. Introduction

The mechanisms of plastic deformation of nanocrystalline materials have been widely studied because of their proved superior functional and mechanical properties.[1-4] The plastic deformation of conventional coarse-grained materials is mainly accommodated by dislocation nucleation and their motion in the interior of grains. However, nanoscale confinement severely limits the operation of traditional dislocation generation mechanisms in nanocrystalline materials. Both experiment[5-7] and molecular dynamics (MD) simulations[8-10] have reported a deviation from traditional Hall-Petch constitutive behavior. Many research works[11-14] indicated that the dislocation activities in the interior of grains lessen when the average grain size is less than 100 nm, whereas mechanisms mediated by the grain boundary (GB) become dominant. For example, small grain size can result in heterogeneous nucleation and emission of dislocations from GBs[15-17]. Yamakov *et al.*[18] proposed a deformation mechanism map that described the transition from dislocation-driven to GB-mediated plastic deformation based on the splitting distance between partial dislocations and the stacking fault energy γ_{sf}. Van Swygenhoven and coworkers[19] revealed that γ_{sf} alone cannot capture the important physics of the nucleation of partial dislocations from GBs, a correct interpretation of the nature of slip in nanocrystalline metals requires the generalized stacking fault energy (GSF) curve that was first introduced by Vitek[20, 21], involving both stable stacking fault energy γ_{sf} and unstable stacking fault energy γ_{usf}.

Study on stacking fault energy can help to better understanding slip behavior in nanocrystalline materials and, thereby, to understand how to improve their mechanical properties.

It is desirable to know the shape of the entire GSF curve to use it in a criterion for nucleation. Since only a single point know as the intrinsic (or stable) stacking fault γ_{sf} can be measured experimentally, many efforts to calculate this curve are based on modeling and simulation methods such as density functional theory (DFT) and molecular dynamics (MD). However, Most of the previous simulation works in calculating GSF are conducted in an undeformed or stress free crystal structures, which is far from the actual situation where the micro or nano-components can be deformed under multiple stress state. The preloading strain or stress on crystal structures are determined to significantly influence the GSF curve. For instance, Zimmerman *et al.*[22] observed that the unrelaxed γ_{usf} value of 175 mJ/m^2 was reduced to 99 mJ/m^2 after biaxially stretch the lattice by 4% when calculating the GSF curve of Cu. Tschopp *et al.*[23] used MD simulations to investigate the influence of normal stress on the GSF curve in Cu, they found that the compressive (tensile) normal stress increases (decreases) the unstable stacking fault energy γ_{usf}, while the stable stacking fault energy γ_{sf} changes in an opposite manner. In addition, the stress influence on GSF curve is not only limited in the normal direction of the slip plane, lateral stress can also influence the value of generalized stacking fault energy. Ogata *et al.*[24] used DFT calculation of stacking fault energy for Al and Cu to study their ideal shear strength. The results indicated that the hydrostatic pressure has a significant effect on the critical resolved shear stress at the atomic scale. Further, Tschopp *et al.*[25, 26] proposed that the stress required for dislocation nucleation depends on both Schmid stress component (resolved shear stress in the slip direction) and non-Schmid stress component (resolved normal stress and resolved shear stress perpendicular to the slip direction) acting on the {1 1 1} slip plane. Our previous work[27, 28] also showed that the effect of stress state can play an important role in dislocation nucleation and fracture of nanocrystalline Cu.

All of the described works show that the GSF curve can be affected by the magnitude and directionality of the applied stress. In the previous study, Rice[29] indicated that unstable stacking fault energy γ_{usf} of the GSF curve was associated with the energy barrier for dislocation nucleation. Tadmor and Hai[30, 31] developed a criterion for the deformation mechanism of mechanical twinning, they found that the 'twinning tendency' was closely related to the unstable twin fault energy γ_{utf} of the GSF curve. In this sense, the energy barrier of both dislocation nucleation and twinning formation in crystals can be influenced by the stress state of crystal lattice. The present work is carrying out MD simulations to investigate the effect of preloading stress with different direction and magnitude on the GSF curve of three fcc metals (Cu, Al and Ni). The unstable stacking fault energy (γ_{usf}), stable stacking fault energy (γ_{sf}) and unstable twin fault energy (γ_{utf}) will be considered.

2. Simulation method

Simulations were performed by the parallel MD code LAMMPS[32]. The embedded atom method (EAM) potential was used in MD simulations. The EAM method defines the total energy of an elemental system which represented as:

$$E_{tot} = \frac{1}{2}\sum_{i \neq j} V(r_{ij}) + \sum_{i} F(\rho_i)$$

Where $V(r_{ij})$ is a pair potential as a function of distance r_{ij} between atoms i and j. $F(\rho_i)$ is the

embedding energy as a function of the host electron density ρ_i induced at site *i* by all other atoms in the system. In this study, EAM potentials developed by Mishin *et al*. for Cu[33], Al[34], and Ni[35] were used. These well-defined potentials were widely used in the MD simulations and they can fit a large set of experimental and first-principles data. For example, the intrinsic (stable) stacking fault energy γ_{sf} and unstable stacking fault energy γ_{usf} of Cu from their simulation result is 44.4 mJ/m^2 and 158 mJ/m^2 respectively[33], which are very close to the experimental measurement 45 mJ/m^2[36] and 162 mJ/m^2.[33] Similarly for Al, Mishin *et al*. reported an intrinsic stacking fault energy of 146 mJ/m^2 and an unstable stacking fault energy of 168 mJ/m^2, both of which are in agreement with the *ab initio* calculations performed in their work.[34]

For calculating GSF using MD, a simulation model was created with [1 1 -2], [1 1 1] and [1 -1 0] directions and it was divided into two blocks in the normal direction (see in Fig.1). A free boundary condition was used in the normal direction ([1 1 1] direction), while a periodic boundary condition was used in the lateral direction ([1 1 -2] and [1 -1 0] direction). This is a similar boundary condition used in Ref.[37] to study the effect of vacancy defects on GSF energy of fcc metals. The GSF curve was determined by rigidly displacing the upper block on a (1 1 1) plane along a [1 1 -2] direction while fixing the lower block and calculating the energy change in the whole simulation model. When displacing the upper block along [1 1 -2] direction, the lateral motion of atoms was constrained. The LAMMPS code for calculating the GSF curve of Cu in this study under stress free condition is given in the Appendix section.

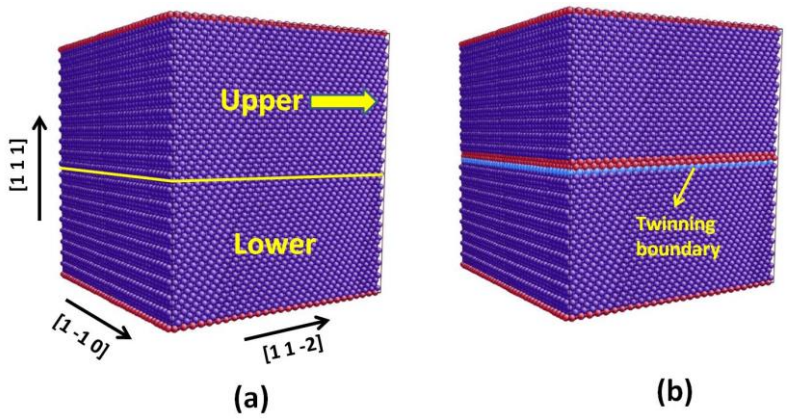

Figure.1 Simulation model for calculating the generalized stacking fault (GSF) energy curve. (a) The starting configuration with perfect fcc lattice. (b) A twinning boundary was formed after rigidly displacing the upper block on a (1 1 1) plane along a [1 1 -2] direction. Atoms with perfect fcc structure are colored with dark blue, the red atoms represent the stacking fault and the free surface, the light blue atoms indicate the twin fault.

For the case of calculating γ_{usf} and γ_{sf}, the starting configuration is a perfect fcc lattice[22, 27](see in Fig.2-a). Along the path, the system will have to first pass through an energy barrier that is referred as unstable stacking fault energy γ_{usf}, the position of the displaced atoms is shown in Fig.2(b). Zimmerman *et al.*[22] indicated that the ideal displacement of the fcc lattice when γ_{usf} reached equals to one-half of the partial Burgers vector $a_0/\sqrt{6}$ (a_0 is the equilibrium fcc lattice parameter). The simulation cell became stable when the displacement is $a_0/\sqrt{6}$, although the cell is not in its bulk equilibrium structure. The configuration in Fig.2(c) is known as the intrinsic stacking fault. Slip in the <1 1 2> direction is common because γ_{usf} is lowest in this direction. For the case of calculating γ_{utf}, the starting configuration is a pre-existing stacking fault.[34]

Specifically, γ_{utf} was calculated by rigidly shifting the block along [1 1 -2] direction in a (1 1 1) plane that is one atom layer above a stacking fault previously formed by shearing, as illustrated in Fig.2(d). Fig.1(b) shows the configuration of simulation cell when a twinning boundary was formed after rigidly displacing the upper block.

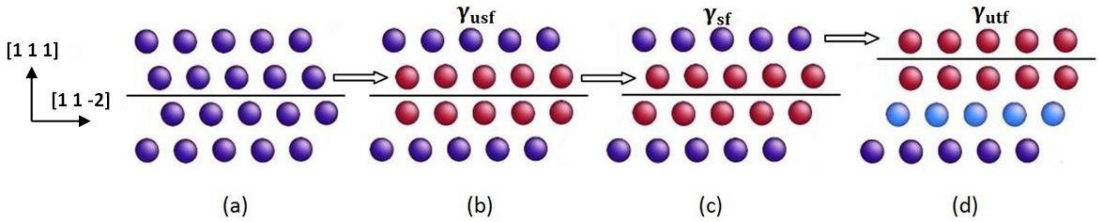

Figure.2 Schematic view of the atom positions when calculating the GSF curve. (a) perfect fcc crystal (b) unstable stacking fault (c) stable stacking fault, and (d) unstable twin fault. Configurations is viewed from the [1 -1 0] direction. Atoms with perfect fcc structure are colored with dark blue, the red atoms represent the stacking fault and the light blue atoms represent the twin fault.

To simulate the influence of stress on the GSF curve, the simulation cell was uniformly strained along one of the following directions: [111], [11-2] and [1-10] with a constant rate of 10^8/s at 1 K before the calculation of the GSF energy in the (111)[11-2] slip system. The high strain rate is inherent in the simulations for computational efficiency to have the desired amount of deformation within a given simulation time. An isobaric-isothermal (NPT) ensemble was used during the uniaxial tensile or compression. While the strain deformation was applied in one direction, the pressure of the lateral directions was kept zero. The system stress was attained by calculating the pressure of the entire system of atoms. The pressure was computed by the formula:

$$P_{ij} = \frac{1}{V}[\sum_k^N m_k v_{k_i} v_{k_j} + \sum_k^N r_{k_i} f_{k_j}] \text{ , } (i \text{ ,} j{=}x \text{ ,} y \text{ ,} z)$$

where the first term uses components of the kinetic energy tensor and the second term uses components of the virial tensor. *N* is the total number of atoms in the simulation model, *V* is the simulation model volume. *r* and *f* is the force vector and the distance vector respectively. System strain was derived from the positions of the periodic boundaries.

3. Results and discussion

Fig.3 plots the stress-strain response of the three investigated fcc metals (Cu, Al and Ni) under uniaxial tension and compression along [1 1 1], [1 1 -2], and [1 -1 0] direction respectively. Notice that, the negative values of compressive stress are plotted in these graphs in order to compare with the values of tensile stress. Obviously, elastic modulus show big differences for different elements. Also, due to the material anisotropy, elastic modulus are slightly different for the same element in different directions. In addition, tension-compression asymmetry in elastic response is evident in all directions. In general, the elastic modulus of compression is higher than the value of tension, and this trend of asymmetry is more obvious for Al than the other two elements. The elastic modulus calculated from the initial slope of the MD simulations are listed in Table-1. Notice that, the nonlinear elastic effect is obvious for Al in [1 -1 0] direction. This nonlinear stress-strain response is due to the non-negligible lattice rotation during elastic deformation at high strain[23].

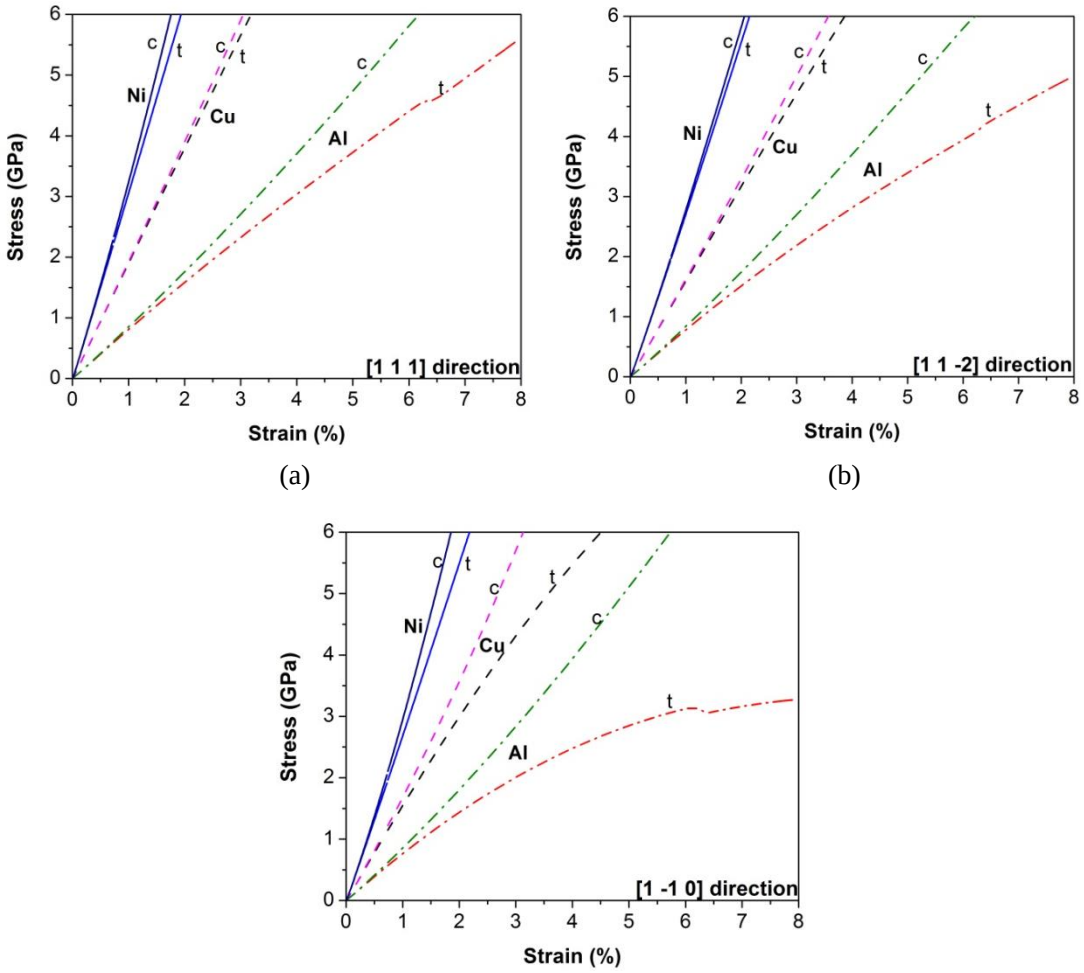

Figure.3 Stress-strain curves for uniaxial tension and compression of Cu, Al and Ni along (a) [1 1 1] direction, (b) [1 1 -2] direction, and (c) [1 -1 0] direction. The negative values of compressive stress are plotted. **t** means uniaxial tension while **c** means uniaxial compression.

Table-1. Elastic modulus calculated from MD simulation

		Elastic Modulus (GPa)		
Element	**Preloading**	$E_{[1\,1\,1]}$	$E_{[1\,1\,-2]}$	$E_{[1\,-1\,0]}$
Cu	Tension	189.8	159.1	154.4
	Compression	192.3	162.0	167.9
Ni	Tension	305.4	270.4	268.2
	Compression	323.4	277.3	294.8
Al	Tension	80.7	78.0	76.1
	Compression	84.9	83.7	85.3

The influence of the preloading stress on the GSF curve of Cu is shown in Fig.4. In the normal [1 1 1] direction and lateral [1 -1 0] direction, the tensile (compressive) stress decreases (increases) the unstable stacking fault energy (γ_{usf}) and the unstable twin fault energy (γ_{utf}), the greater the magnitude of the preloading stress, the greater the decreases (increases) of the value. However, the stable stacking fault energy (γ_{sf}) changes in an opposite manner in [1 1 1] direction. γ_{sf} increases under the preloading tensile stress and decreases under the compressive stress. The effect is more noticeable at higher stress of compression. For example, γ_{sf} increases 4.9% at 5 GPa tensile stress and decreases 17.5% at 5 GPa compressive stress. Different from the cases in [1

1 1] and [1 -1 0] directions, the tensile stress increase the value of γ_{usf} and γ_{utf} in [1 1 -2] direction while the compressive stress decreases the values. It is interesting to note that, under the preloading stress in all directions, the value of γ_{usf}, γ_{sf} and γ_{utf} may reached before or after their ideal displacement, a value that can be expected from geometric considerations. Ideally in the figures, $\delta_{sf}=\frac{1}{2}a_0/\sqrt{6}$, $\delta_{usf}=a_0/\sqrt{6}$, $\delta_{utf}=\frac{3}{2}a_0/\sqrt{6}$, where a_0 is the equilibrium fcc lattice parameter. This deviation is mainly due to the pre-strain changes the interatomic distance of the equilibrium structure.

Fig.5 shows the effect of stress on the GSF curve of Ni. In general, the influence of tensile and compressive stress on the GSF curve of Ni in all directions is similar to the stress effect on Cu. In [1 1 1] and [1 -1 0] directions, γ_{usf} and γ_{utf} decreases (increases) with the increased magnitude of tensile and compressive stress, while the tensile and compressive stress effect in an opposite way in [1 1 -2] direction. The influence of the preloading stress on GSF curve of Ni is not as obvious as that of Cu, and the deviation of the ideal displacement when each value reached is less than that of Cu. This is due to the higher elastic modulus of Ni than Cu (see in Fig.3), i.e. lattice deformation and the change of the interatomic distance is less in Ni than Cu at the same value of the applied stress.

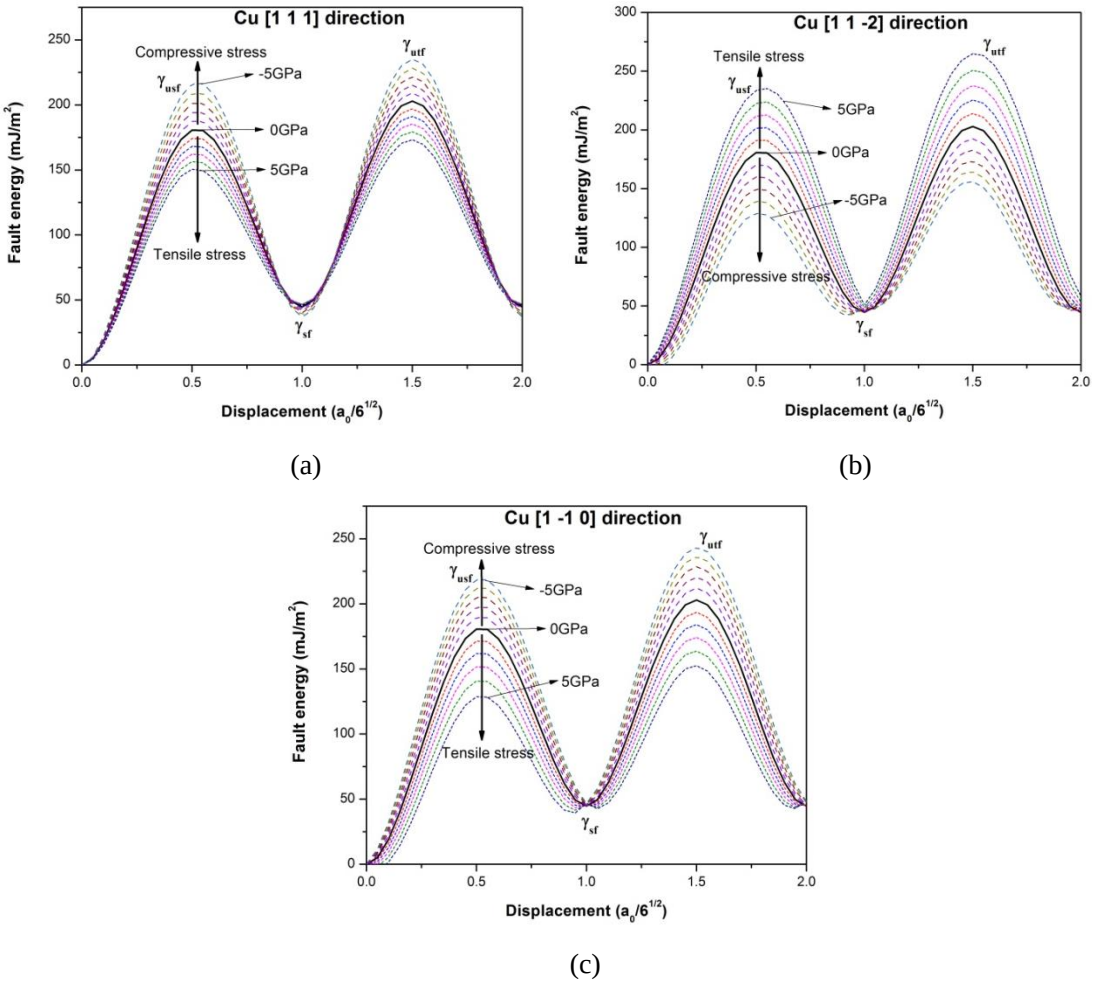

Figure.4 Influence of stress on the generalized stacking fault energy curve in Cu. The tensile and compressive stress was applied along (a) [1 1 1] direction, (b) [1 1 -2] direction, and (c) [1 -1 0] direction.

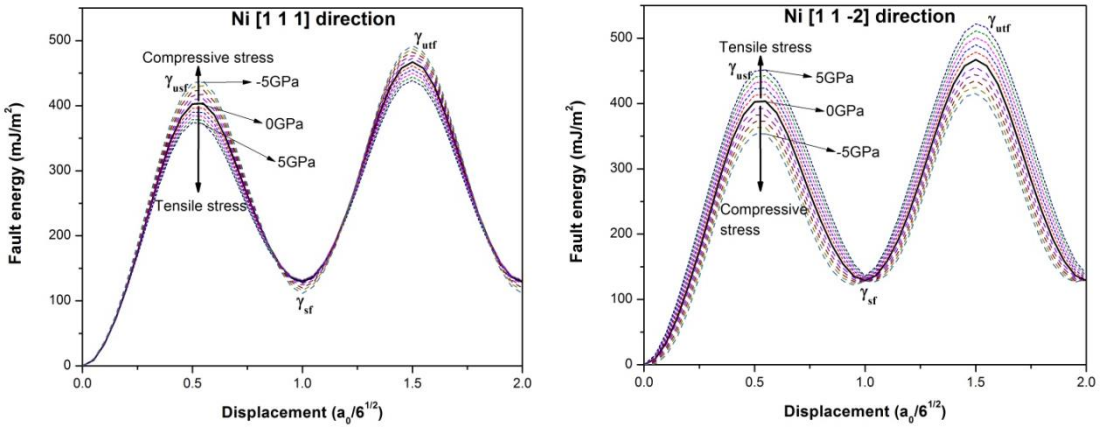

(a)

(b)

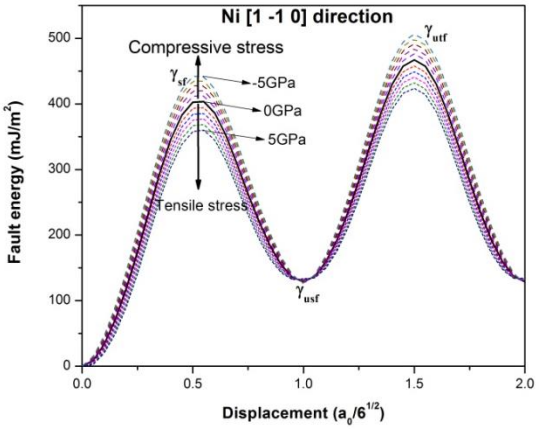

(c)

Figure.5 Influence of stress on the generalized stacking fault energy curve in Ni. The tensile and compressive stress was applied along (a) [1 1 1] direction, (b) [1 1 -2] direction, and (c) [1 -1 0] direction.

For Cu and Ni, the preloading stress has an obvious influence on the value of γ_{usf} and γ_{utf}, while the influence on the value of γ_{sf} is limit. However, this is not the case of Al, the preloading stress can greatly influence on the three values in all directions, especially in the normal [1 1 1] direction. Fig.6 shows the influence of tensile and compressive stress on the GSF curve of Al. In Fig.6(a), the value of γ_{usf}, γ_{sf} and γ_{utf} increases for 41.2%, 59.8% and 43.3% at 5 GPa compressive stress and drops sharply for 53.5%, 82.7% and 59.4% respectively at 5 GPa tensile stress. Another difference of Al from Cu and Ni in the GSF curve is observed in [1 -1 0] direction. In Fig.4(c) and Fig.5(c), γ_{usf} and γ_{utf} decrease in tension and increase in compression, while in Fig.6(c), this effect acts in an opposite manner. In addition, the applied tension stress plays a little role on the value of γ_{usf} and γ_{utf} in [1 -1 0] direction, 1.1% and 2.3% increase respectively at 3 GPa tensile stress. Moreover, the value of different fault energies can changes faster at a higher tensile stress in [1 1 -2] and [1 -1 0] directions due to the nonlinear elastic effect in these directions of Al.

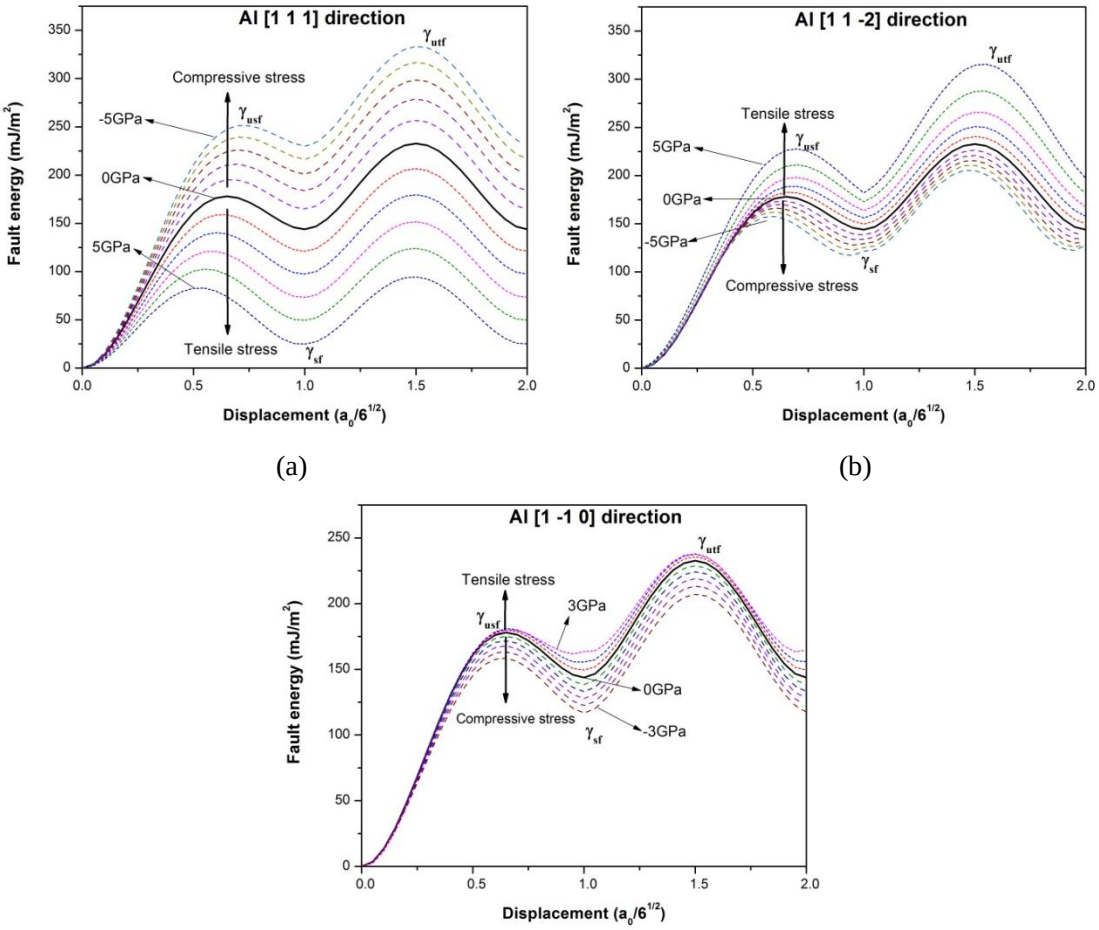

Figure.6 Influence of stress on the generalized stacking fault energy curve in Al. The tensile and compressive stress is applied along (a) [1 1 1] direction, (b) [1 1 -2] direction, and (c) [1 -1 0] direction.

In previous studies, MD simulations have revealed that the small gain size in nanocrystalline materials can result in the heterogeneous nucleation and emission of dislocations from the GBs. The deformation mechanism has been confirmed by recent *in situ* transmission electron microscopy experiments in nanocrystalline Al[38] and Cu[39]. The experiments have also shown that stacking faults and deformation twins can be formed through partial dislocation emission from GBs. Van Swygenhoven *et al.*[19] indicated that all aspects of the GSF curve have to be incorporated to well understand the slip activities observed in simulations, the deformation cannot be explained by means of the absolute value of γ_{sf} alone as suggested by Yamakov *et al.*[18]. Specifically, whether extended partial dislocations or full dislocations travelling through the grains dominates the deformation mechanism in a simulation must understood in terms of the ratio γ_{sf}/γ_{usf}. This value closer to unity is associated with fcc materials that nucleate full dislocations.

Fig.7 shows the ratio γ_{sf}/γ_{usf} changes as a function of the preloading stress in different directions. For the case of Cu and Ni, the applied tensile stress increases the value while the compressive stress decreases the value in [1 1 1] and [1 -1 0] directions. In [1 1 -2] direction, this effect acts in an opposite manner. Overall, the influence of the applied stress on the value of γ_{sf}/γ_{usf} for Cu and Ni is not obvious. The value is at a relatively low level (ranged from 0.17 to 0.33 for Cu and 0.26 to 0.37 for Ni), which means the nucleation of partial dislocation and its propagation in the grain is still the dominant mechanism in nanocrystalline Cu and Ni even in a

condition of high stress concentration.

For the case of Al, the ratio γ_{sf}/γ_{usf} decreases significantly with the increase of the preloading tensile stress in [1 1 1] direction (see in Fig.7-a). At 5 GPa tensile stress, the ratio drops to the same level as Cu and Ni. The sharp decrease of γ_{sf}/γ_{usf} indicates that the nucleation of full dislocation (with trailing partial dislocation) that observed in simulations of Al[17, 19] may be restricted under tensile stress that applied normal to the slip plane, i.e. the extended partial dislocation may dominate the deformation mechanisms as same as the case of Cu and Ni. In addition, the applied compressive stress in [1 1 1] direction and tensile stress in [1 -1 0] direction increases the ratio γ_{sf}/γ_{usf} to a level more closer to unity, as shown in Fig.7(a) and (c). It means that the trailing partial dislocations can nucleate more easily and the separation of the leading and trailing partials will be shortened. The effect of stress in [1 1 -2] direction on the ratio γ_{sf}/γ_{usf} is not obvious, ranged from 0.74 to 0.83.

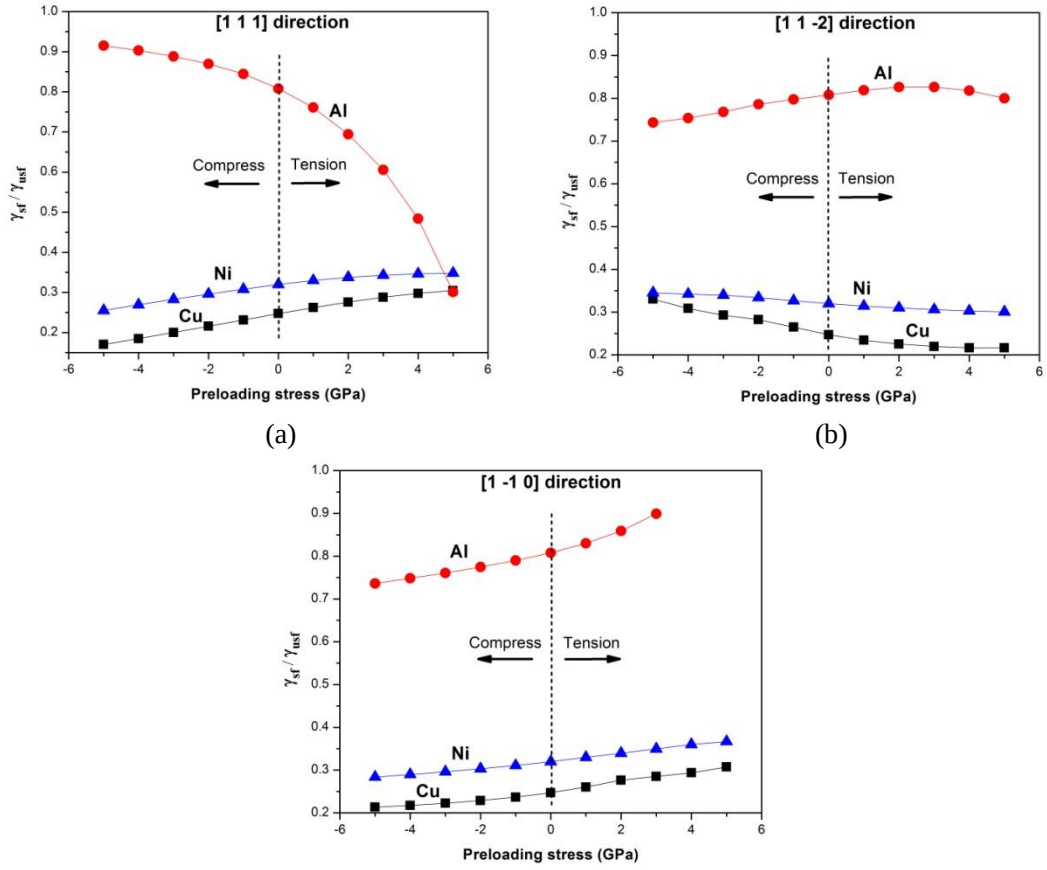

Figure.7 The ratio of stable stacking fault energy to unstable stacking fault energy (γ_{sf}/γ_{usf}) as a function of the preloading stress along (a) [1 1 1] direction, (b) [1 1 -2] direction, and (c) [1 -1 0] direction.

As previously reported [30, 31], the observation of twinning nucleation in a simulation is depend on the ratio $\gamma_{utf}/\gamma_{usf}$, where γ_{utf} relates to the energy barrier for twinning formation and γ_{usf} is associated with the barrier for a full dislocation nucleation. The ratio controls the competition of the two possible mechanisms. γ_{utf} is larger than γ_{usf} in all cases of our simulation for the GSF curve, which is consistent with the results of Van Swygenhoven *et al.*[19] by testing the GSF curves with different EAM potentials. This can explain why mechanical twinning is not observed as the dominant mechanisms in most of the MD simulations of nanocrystalline samples with defect-free

grains, since it will overcome greater energy barrier. The influence of the applied stress on the ratio $\gamma_{utf}/\gamma_{usf}$ is shown in Fig.8. In general, the value of $\gamma_{utf}/\gamma_{usf}$ for Cu is at the lowest level of all the three tested elements, and this value is more closer to unity when compressive stress applied normal to the slip plane (see in Fig.8-a). It means that the barrier for twinning formation and for dislocation nucleation is comparable and twinning is easier to grow in Cu in certain conditions. For example, Lu and collaborates[40] used the nanoscale growth twins in Cu sample to effectively increase its strength. The applied tensile stress in [1 1 1] and [1 -1 0] directions and the compressive stress in [1 1-2] direction increases the value of $\gamma_{utf}/\gamma_{usf}$ for Cu so that increases the difficulty of twinning formation. For the case of Ni, the effect of stress on the ratio $\gamma_{utf}/\gamma_{usf}$ is not significant in all directions, this value ranges from 1.13 to 1.18.

The value of $\gamma_{utf}/\gamma_{usf}$ for Al is much higher than the value of Cu and Ni, so the twinning is more difficult to form in Al. However, the tensile stress in [1 1 1] direction can sharply decrease the value, from 1.31 in stress free condition to 1.14 at 5 GPa preloading stress. The sharp decrease of $\gamma_{utf}/\gamma_{usf}$ indicates that twinning may also observed as a deformation mechanism in high stress concentration condition, especially when the applied tensile stress has a high component normal to the slip plane. For example, twinning deformation mechanism has been observed in the experiments[38, 39], in which twin boundary nucleation becomes favorable over full dislocation nucleation when high shear stress are provided (for example, during ball milling and high-pressure torsion). The tensile stress in [1 1 -2] and [1 -1 0] direction increases the value of $\gamma_{utf}/\gamma_{usf}$ for Al so that can increase the difficulty of twinning formation.

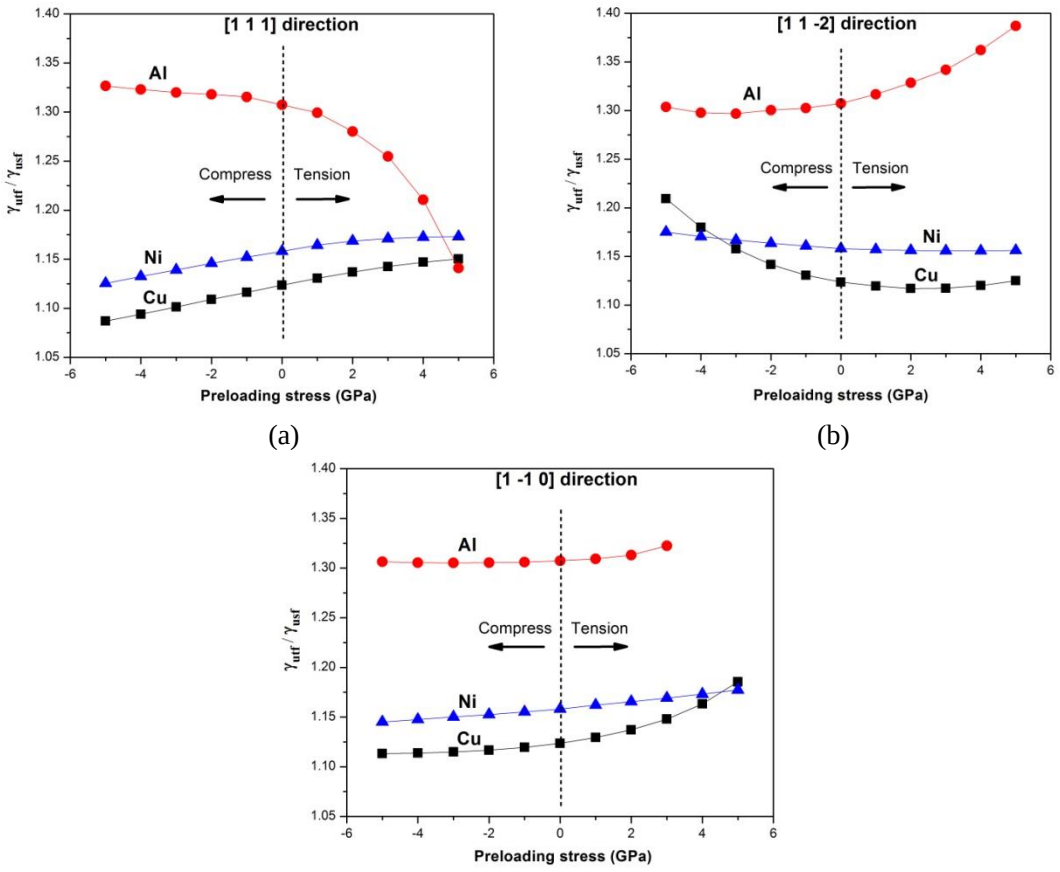

Figure.8 The ratio of unstable twin fault energy to unstable stacking fault energy $\gamma_{utf}/\gamma_{usf}$ as a function of the preloading stress along (a) [1 1 1] direction, (b) [1 1 -2] direction, and (c) [1 -1 0] direction.

4. Conclusion

MD simulations were used to investigate the influence of tensile and compressive stress on (1 1 1)[1 1 -2] GSF energy curves in [1 1 1], [1 1 -2] and [1 -1 0] directions for three different fcc metals. The widely used EAM potentials developed by Mishin for Cu[33], Al[34], and Ni[35] were tested in this study. Simulation results show that GSF curves of the three elements can be influenced by the preloading stress. The value of γ_{usf}, γ_{sf} and γ_{utf} increased or decreased when preloading tensile or compressive stress was applied in certain direction. The effect of stress on the ratio of γ_{sf}/γ_{usf} and $\gamma_{utf}/\gamma_{usf}$, which are closely related to the deformation mechanisms in nanocrystalline materials, were also investigated in this study. The results quantitatively demonstrate that not only the resolved stress along the slip plane (traditional Schmid factor), but also the resolved stress normal to the slip plane and the resolved stress perpendicular to the slip direction can play an important role in dislocation nucleation and twinning formation. The change in the GSF energy curve as a function of the applied stress indicates that the stress state is another important factor that can influence the deformation mechanisms of nanocrystalline materials.

Acknowledgements

L. Zhang, X. Zhao and L.Q. Pei would like to acknowledge the financial support from China Scholarship Council (CSC).

Appendix

```
### LAMMPS code for calculating the GSF energy curve of Cu
### file_name    in.gsf-cu

units           metal
boundary        p s p
atom_style      atomic
variable        lattice equal 3.615
variable        partial equal "v_lattice/sqrt(6)"
variable        cna equal "v_lattice*(1+1/sqrt(2))/2"

lattice         fcc ${lattice} orient x 1 1 -2 orient y 1 1 1 orient z 1 -1 0
region          box block 0 21 0 20 0 20
create_box      1 box
create_atoms    1 box

region          up1 block INF INF 62 INF INF INF units box
group           up1 region up1

region          up2 block INF INF 64 INF INF INF units box
group           up2 region up2

region          energy block INF INF 45 80 INF INF units box
group           energy region energy

neighbor        2.0 bin
neigh_modify    delay 1 check yes
pair_style      eam/alloy
pair_coeff      * * Cu01.eam.alloy Cu
```

```
compute         pe all pe/atom
compute         cna all cna/atom ${cna}
mass            * 63.546

compute         gbenergy energy reduce sum c_pe
variable        gbenergy equal c_gbenergy

thermo          1
thermo_style    custom step temp pe ke etotal lx ly lz pxx pyy pzz c_gbenergy
dump            1 all cfg 1 cell.*.cfg id type    xs ys zs c_cna c_pe
dump_modify     1 element Cu
dump            2 energy cfg 1 gsf.*.cfg id type    xs ys zs c_cna c_pe
dump_modify     2 element Cu
run             0

variable        gbenergy00 equal "v_gbenergy"
variable        gbenergy0 equal ${gbenergy00}

label           forloopp
variable        a loop 20
variable        p equal "v_partial/20"
displace_atoms  up1 move ${p} 0 0 units box
variable        gsf equal "(v_gbenergy-v_gbenergy0)/lx/lz*16.02*1000"
fix             extra all print 1 "$a ${gsf}" append data.gsf-Cu-0 screen no title a
run             1
next            a
jump            in.gsf-cu forloopp

label           forloopt
variable        a loop 21 40
variable        p equal "v_partial/20"
displace_atoms  up2 move ${p} 0 0 units box
variable        gsf equal "(v_gbenergy-v_gbenergy0)/lx/lz*16.02*1000"
fix             extra all print 1 "$a ${gsf}" append data.gsf-Cu-0 screen no title a
run             1
next            a
jump            in.gsf-cu forloopt
```

References

1. Champion Y, Langlois C, Guérin M S, Langlois P, Bonnentien J L and Hÿtch M J 2003 *Science* **300** 310
2. Lu L, Shen Y, Chen X, Qian L and Lu K 2004 *Science* **304** 422
3. Ma E 2003 *Nature Mater.* **2** 7
4. Schiøtz J and Jacobsen K W 2003 *Science* **301** 1357
5. Zhou Y, Erb U, Aust K T and Palumbo G 2003 *Scr. Mater.* **48** 825
6. Wang Y M, Hamza A V and Ma E 2005 *App. Phys. Lett.* **86** 241917
7. Wang Y M, Hamza A V and Ma E 2006 *Acta Mater.* **54** 2715
8. Schiøtz J, Tolla F D and Jacobsen K W 1998 *Nature* **391** 561
9. Schiøtz J, Vegge T, Tolla F D and Jacobsen K W 1999 *Phys. Rev. B* **60** 11971
10. Schiøtz J 2004 *Scr. Mater.* **51** 837
11. Asaro R J, Krysl P and Kad B 2003 *Philos. Mag. Lett.* **83** 733
12. Koch C C 2003 *Scr. Mater.* **49** 657

13. Kumar K S, Van Swygenhoven H and Suresh S 2003 *Acta Mater.* **51** 5743
14. Van Swygenhoven H 2002 *Science* **296** 66
15. Tschopp M A and McDowell D L 2008 *Int. J. Plast.* **24** 191
16. Spearot D E, Jacob K I and McDowell D L 2007 *Int. J. Plast.* **23** 143
17. Spearot D E, Jacob K I and McDowell D L 2005 *Acta Mater.* **53** 3579
18. Yamakov V, Wolf D, Phillpot S R, Mukherjee A K and Gleiter H 2004 *Nature Mater.* **3** 43
19. Van Swygenhoven H, Derlet P M and Frøseth A G 2004 *Nature Mater.* **3** 399
20. Vítek V 1966 *Phys. Status Solidi* **18** 687
21. Vítek V 1968 *Philos. Mag.* **18** 773
22. Zimmerman J A, Gao H and Abraham F F 2000 *Modell. Simul. Mater. Sci. Eng.* **8** 103
23. Tschopp M A and McDowell D L 2008 *J. Mech. Phys. Solids.* **56** 1806
24. Ogata S, Li J and Yip S 2002 *Science* **298** 807
25. Tschopp M A, Tucker G J and McDowell D L 2008 *Comput. Mater. Sci.* **44** 351
26. Spearot D E, Tschopp M A, Jacob K I and McDowell D L 2007 *Acta Mater.* **55** 705
27. Zhang L, Lu C and Tieu K 2014 *Sci. Rep.* **4** 5919
28. Zhang L, Lu C, Tieu K, Pei L Q and Zhao X 2014 *Chin. Phys. B* **23** 98102
29. Rice J R 1992 *J. Mech. Phys. Solids.* **40** 239
30. Hai S and Tadmor E B 2003 *Acta Mater.* **51** 117
31. Tadmor E B and Hai S 2003 *J. Mech. Phys. Solids.* **51** 765
32. Plimpton S 1995 *J. Comput. Phys.* **117** 1
33. Mishin Y, Mehl M J, Papaconstantopoulos D A, Voter A F and Kress J D 2001 *Phys. Rev. B* **63** 2241061
34. Zope R R and Mishin Y 2003 *Phys. Rev. B* **68** 024102
35. Mishin Y, Farkas D, Mehl M J and Papaconstantopoulos D A 1999 *Phys. Rev. B* **59** 3393
36. Carter C B and Ray I L F 1977 *Philos. Mag.* **35** 189
37. Ebrahim A., Mohsen Asle Z, Amitava M and Mark A T 2014 *J. Phys.:Condensed Matter.* **26** 115404
38. Liao X Z, Zhou F, Lavernia E J, He D W and Zhu Y T 2023 *Appl. Phys. Lett.* **75** 5062
39. Liao X Z, Zhao Y H, Srinivasan S G, Zhu Y T, Valiev R Z and Gunderov D V 2004 *Appl. Phys. Lett.* **75** 592
40. Lu K, Lu L, Chen X and Huang X 2009 *Science* **323** 607